Korean J. Chem. Eng., **19**(5), 749-755 (2002)

Electrochemical Characteristics of Lithium Transition-Metal Oxide as an Anode Material in a Lithium Secondary Battery

Chil-Hoon Doh†, Bong-Soo Jin, Jung-Hwan Lim* and Seong-In Moon

Battery Research Group, Advanced Materials and Application Laboratory Research,
Korea Electrotechnology Research Institute (KERI), Changwon 641-120, Korea
(*Received 8 March 2001 • accepted 8 May 2002*)

Abstract−Lithium transition-metal oxides (LiTMOs) such as $LiCoO_2$ and $LiMn_2O_4$ were investigated for their use as anode material for the lithium secondary battery. $Ni|Li^0|LiPF_6$(1M, EC + DEC (1 : 1))|LiTMO|Cu cell was fabricated and its electrochemical properties were examined. $LiCoO_2$ and $LiMn_2O_4$ showed fairly good characteristics as anode material as well as cathode material. At the 1st cathodic process, $LiCoO_2$ had a potential plateau at 1.4 V on open circuit potential line, but $LiMn_2O_4$ had two ambiguous potential plateaus between 0.6 and 0.1 V. The specific resistance of $Li|LiCoO_2$ cell was 8 ohm·g, but that of $Li|LiMn_2O_4$ cell decreased gradually while the reaction proceeded. The specific capacities of $Li|LiCoO_2$ and $Li|LiMn_2O_4$ cells at the 1st discharge were about 300 mAh/g. Capacity retention of $Li|LiMn_2O_4$ cell during charge-discharge cycling was higher than that of $Li|LiCoO_2$ cell.

Key words: $LiMn_2O_4$, $LiCoO_2$, Anode Material, Lithium, Battery

INTRODUCTION

A conventional lithium secondary battery is generally composed of transition-metal oxide cathode, organic carbonate electrolyte containing lithium salt [Doh et al., 2000], and carbon anode such as coke and graphite [Doh et al., 2000]. Lithium metal and lithium-aluminum alloy have been studied as anode materials for the lithium secondary battery. However, Li and Li-Al alloys have not been commercialized due to their poor cycling characteristics and thermal instability [Dahn et al., 1994]. Carbon material, in which lithium ion intercalated electrochemically, is presently commercialized as an anode for the lithium secondary battery.

Recently, new high-capacitive materials such as poly para-phenylene (PPP) [Dubois et al., 1998], polyacene (PAS) [Yamabe et al., 1997], and metal oxides (SnO_x [Idota et al., 1995, 1997], etc.) have been developed in order to overcome the capacity limit of the carbon anode. Tarascon et al. [Poizot et al., 2000] found that transition-metal oxide could be used as the anode material in the lithium secondary battery. They reported that the specific capacities of Co_3O_4 and CoO are 950 mAh/g and 700 mAh/g, respectively.

In this work, we employed the lithium transition-metal oxides (LiTMOs) of $LiCoO_2$ and $LiMn_2O_4$ as cathode materials [Sun and Kim, 1999; Sun et al., 1998], and the electrochemical properties of the materials were characterized to evaluate their usage as an anode material for the lithium secondary battery.

EXPERIMENTAL

$LiCoO_2$ and $LiMn_2O_4$ were used as active materials in the anode. Table 1 shows the properties of active materials used in this study. We explored $LiMn_2O_4$ (Allied Signal Co.) as AS-$LiMn_2O_4$ and $LiMn_2O_4$ (Suttong Co.) as STC-$LiMn_2O_4$, respectively.

Table 1. Properties of active materials

Active material	$LiCoO_2$	AS-$LiMn_2O_4$ ($Li_{1.04}Mn_2O_{4.09}$)	STC-$LiMn_2O_4$
Surface area (m^2/g)	0.51	1.5	2.0
Average particle size (μm)	5	28	5
Tap density (g/cm^3)	-	1.8	2.0
Supplier	Sumitomo Co.	Allied Signal Co.	Suttong Co.

Table 2. Composition of electrode

Active material	Composition of electrode
$LiCoO_2$	$LiCoO_2$: Lonza KS6 : PVDF=83.3 : 12.5 : 4.2 wt%
AS-$LiMn_2O_4$	$LiMn_2O_4$: SGO1 : SPB : PVDF=86 : 4 : 4 : 6 wt%
	$LiMn_2O_4$: VGCF : SPB : PVDF=92 : 2 : 2 : 4 wt%
STC-$LiMn_2O_4$	$LiMn_2O_4$: SGO1 : SPB : PVDF=92 : 2 : 2 : 4 wt%
	$LiMn_2O_4$: VGCF : SPB : PVDF=92 : 2 : 2 : 4 wt%

SGO1 (graphite), SPB (super p black), and VGCF (vapor grown carbon fiber) were used as a conductive material. PVDF (polyvinylidene fluoride) homopolymer (Aldrich Chem. Co.) was used as a binder. The active material, conductive material, and binder were mixed with a composition described in Table 2 and agitated with Zirconia ball and NMP (N-methylpyrrolidone) dispersive solvent to obtain a fine slurry. The obtained slurry was coated on the copper film, and then dried at 120 °C in an oven. This prepared electrode sheet was compressed by twin roll presses, and then cut in a dimension of 20×40 mm^2.

The prepared LiTMO electrode, a counter electrode of lithium foil, and a separator of porous polyethylene were rolled up to make a so-called jelly roll. Three electrode test cells [Doh et al., 1999] were prepared by using a jelly roll, Li/Li^+ reference electrode, and

†To whom correspondence should be addressed.
E-mail: chdoh@keri.re.kr
*Present address: LG Chemicals

1 M $LiPF_6$ electrolyte in EC (ethylene carbonate)+DEC (diethyl carbonate) (1 : 1 vol%) in a glove box.

Electrochemical characteristics of the assembled Li|$LiPF_6$(org.)|LiTMO cells were evaluated by Toscat charge-discharge tester.

X-ray diffractograms and SEM photographs were measured by PW 1830 model of Phillips X-ray diffraction using CuKα radiation monochromated by nickel filter with 0.5°/min scan rate and S-2700 model of Hitachi scanning electron microscopy, respectively.

RESULTS AND DISCUSSION

1. XRD and SEM Analyses

The lattice constants a and c of $LiCoO_2$ were 2.814 Å and 14.045 Å, respectively, and $LiCoO_2$ had hexagonal crystal structure. The lattice constants of AS-$LiMn_2O_4$ and STC-$LiMn_2O_4$ were 8.233 Å and 8.198 Å, respectively. The $LiMn_2O_4$ had spinel crystal structure. Fig. 1 shows XRD patterns obtained from AS-$LiMn_2O_2$ and STC-$LiMn_2O_4$, respectively.

Fig. 2 shows the morphology of AS-$LiMn_2O_4$ obtained by using SEM. The small-size particles were agglomerated in AS-$LiMn_2O_4$ as shown in Fig. 2a and 2b. Average particle size was D_{50} 28.7 μm with D_{10} 13.5 μm and D_{90} 52 μm as shown in Fig. 3. However, these small-sized particles were not observed after the electrode fabrication as shown in Fig. 4.

2. Anode Characteristics for Lithium Secondary Battery

2-1. $LiCoO_2$

It was well known that Li-Al alloy could be formed when aluminum was used as a cathode current collector and its potential was near 0 V vs. Li|Li^+. Li|$LiCoO_2$ and Li|$LiMn_2O_4$ cells had the potential plateau between 0-1.5 V. The potential plateau of these cells was somewhat different from that of Li-Al alloy formation. Electrochemical properties of $LiCoO_2$ were evaluated as an anode. In this case, copper was used as the current collector because Al-Li alloy could be formed when aluminum was used as the current collector material.

A Li|$LiCoO_2$ cell was tested with a scan rate of 0.1 mV/sec at the potential range of 0-3 V vs. Li|Li^+ by cyclic voltammetry as shown

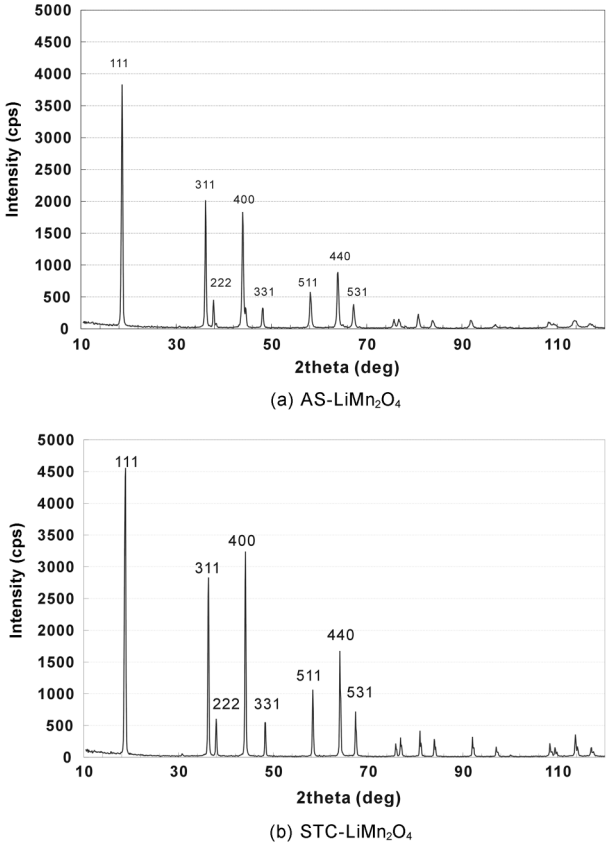

Fig. 1. XRD patterns of AS-$LiMn_2O_4$ and STC-$LiMn_2O_4$ material.

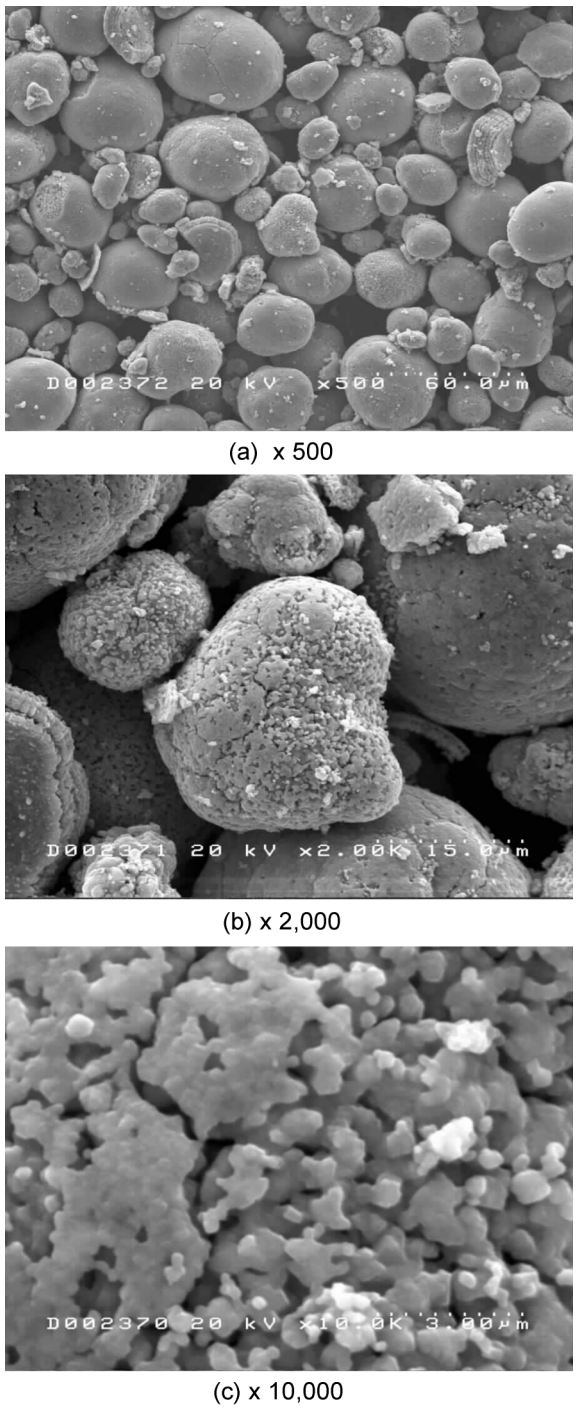

Fig. 2. SEM images of AS-$LiMn_2O_4$ material.

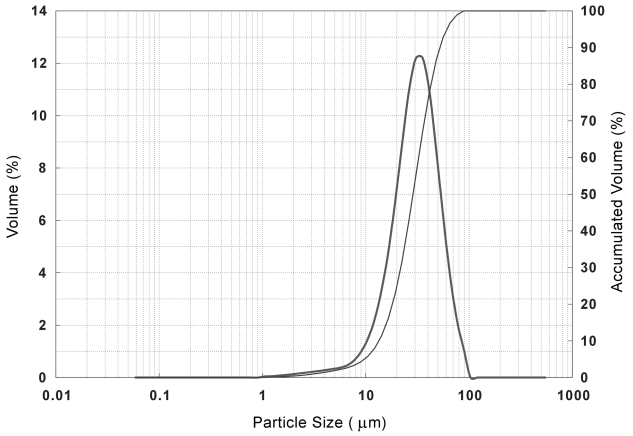

Fig. 3. Particle size distribution of AS-$LiMn_2O_4$ material.

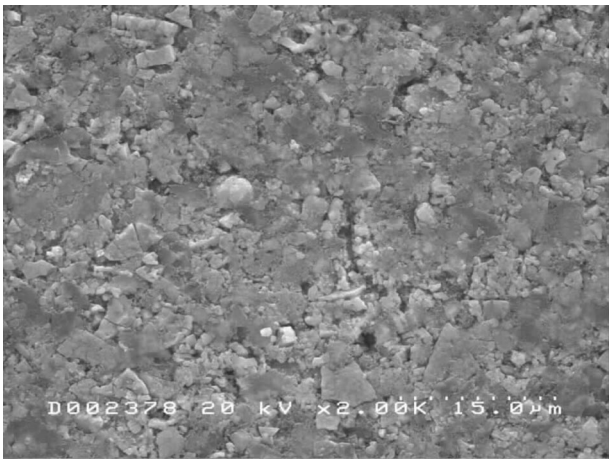

Fig. 4. SEM images of AS-$LiMn_2O_4$ electrode (×2,000); $LiMn_2O_4$: SGO1 : SPB : PVDF=86 : 4 : 4 : 6 wt%.

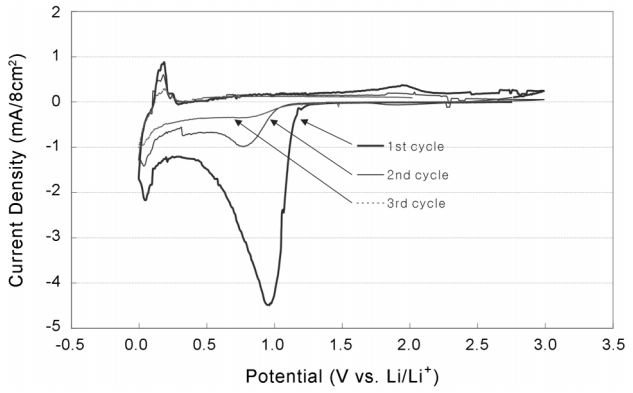

Fig. 5. Cyclic voltammogram of $LiCoO_2$/Li cell. Scan rate; 0.1 mV/sec, potential range; 0-3 V vs. Li/Li^+, material loading; 8 mg/cm^2 on single side.

in Fig. 5. During the 1st cathodic scan, current density increased from ca. 1.2 V, peak current was observed at 1.0 V, and current increased again at 0 V. During the anodic scan, the peak current was observed at 0.17 V due to the dissolution of deposited lithium formed during the cathodic scan. The peak current at 2.0 V corresponded

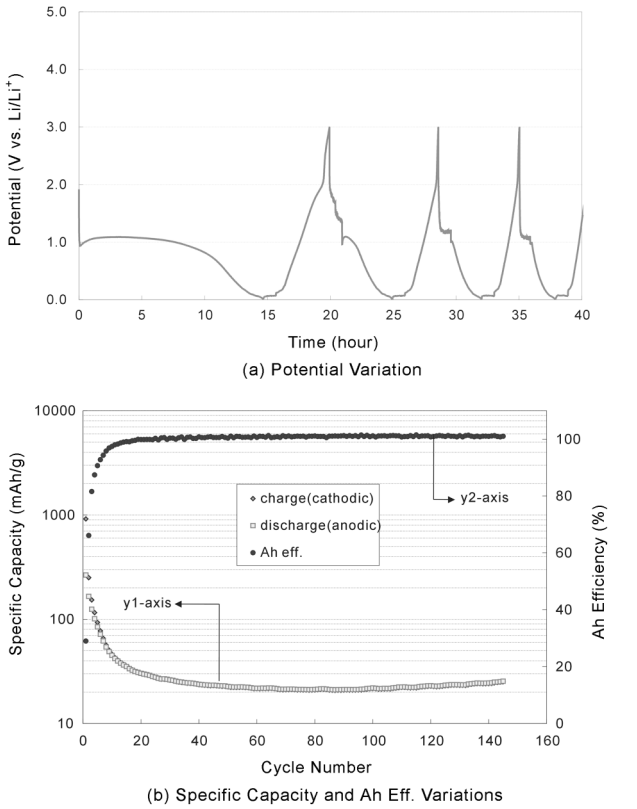

Fig. 6. Charge-discharge characteristics of $LiCoO_2$/lithium cell. Current density; 0.5 mA/cm_2, potential range; 0-3 V vs Li/Li^+, rest; 30 minutes.

to that of 1.0 V in the cathodic scan, indicating a reversible electrochemical reaction. During the cathodic scan after the 2nd cycle, the cathodic current increased from 1.0 V and the peak current was observed at 0.75 V. Therefore, the cathodic process after the 2nd cycle was different from that of the 1st cycle.

The cell properties of a fresh Li|$LiCoO_2$(Cu) cell were evaluated galvanostatically at a current density of 0.5 mA/cm^2 and a potential range of 0.01-3 V using the charge-discharge tester. The results are shown in Fig. 6a. At the initial charge of the 1st cycle, the potential decreased drastically from the open circuit potential of 3 V to 1.0 V and then a potential plateau was observed at 1.1 V. Thereafter, the potential decreased with proceeding charge. The specific capacity at the 1st charge and discharge was 917 mAh/g-$LiCoO_2$ and 266 mAh/g-$LiCoO_2$, respectively. The Ah efficiency at the 1st cycle was 29%. Potential behavior of the discharge step (anodic scan) was different from that of the charge step (cathodic scan). Potential plateau near 1.1 V disappeared after the 2nd charge, but the potential varied in the same region.

Fig. 6b shows the specific capacity and the Ah efficiency plot as a function of charge-discharge cycling. The specific capacity decreased to 20 mAh/g at 80th cycle, and then increased to 25 mAh/g at 140th cycle. However, the Ah efficiencies were almost 100% by the reversible redox reaction.

A fresh Li|$LiCoO_2$ cell was tested by using GITT (galvano-static intermittent transient technique) to obtain O.C.P. (open circuit potential, bold line) and C.C.P. (closed circuit potential, dotted line) curves as shown in Fig. 7a. A potential plateau was observed at 1.3 V

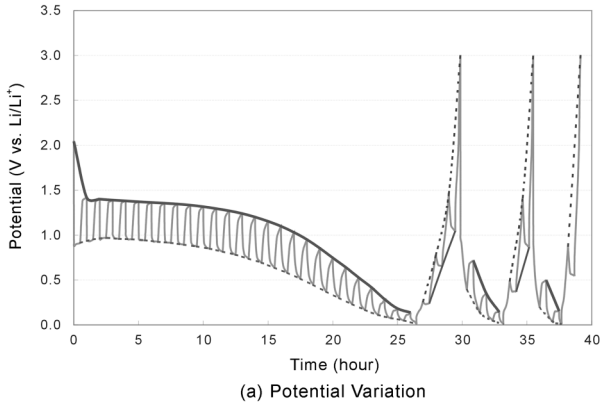

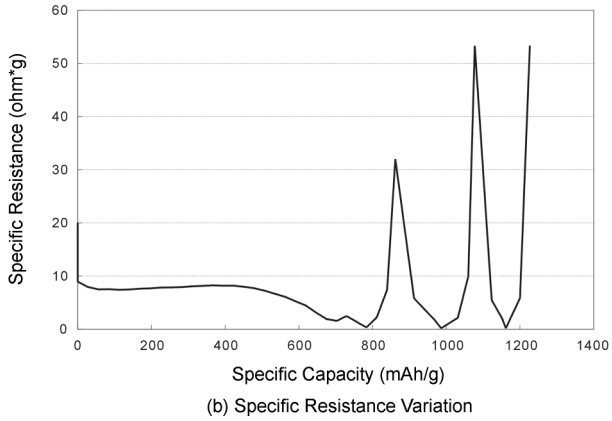

Fig. 7. Intermittent charge-discharge characteristics of $LiCoO_2$/lithium cell. Current density; 0.5 mA/cm^2, potential range; 0-3 V vs Li/Li$^+$, current on; 30 minutes, current off; 30 minutes, charge per one pulse; 28 mAh/g.

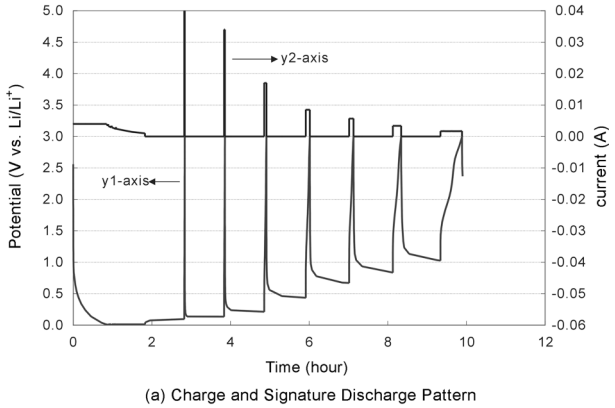

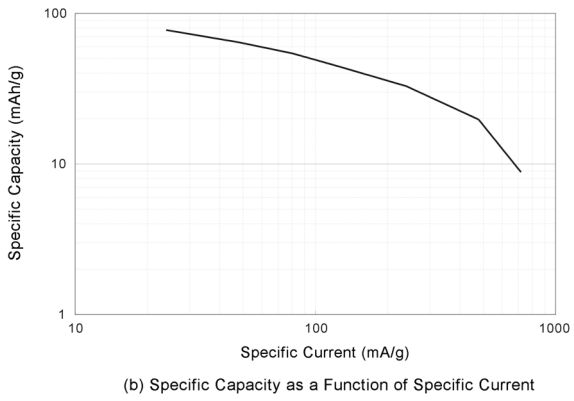

Fig. 8. Drain capability of $LiCoO_2$ cell obtained by using the signature discharge technique.

on the O.C.P. curve. The potential plateau was observed only at the 1st charge. It was thought that reversible reaction occurred after the 1st discharge because the O.C.P. line was symmetrical after the 2nd cycle. The specific resistance, which was obtained from Fig. 7a, was plotted as a function of the specific capacity in Fig. 7b. There were two regions in the specific resistance profile at the 1st charge: irreversible region in which the specific resistance was 8 ohm·g and reversible region in which the specific resistance varied gradually.

Fig. 8a shows the current and the potential plot as a function of the discharge time. Fig. 8a was obtained by signature discharge technique using the tested cell at GITT test. Fig. 8b shows the specific capacity plot as a function of the specific current obtained from the results of Fig. 8a. The specific capacity increased with decrement of the specific current; the specific capacities were 33 and 80 mAh/g at the specific current of 220 and 22 mA/g, respectively. The capacity fading with the charge-discharge cycling made low specific capacity, as shown in Fig. 6b. Potential behavior at the current density of 0.09 and 0.05 mA/cm^2 was similar to that shown in Fig. 8. The 1st charge-discharge results obtained from different current densities are summarized in Table 3. The charge capacity increased a little with decreasing the current density, but the specific discharge capacity increased more rapidly than the specific charge capacity. However, the irreversible specific capacity was sustained at 610-660 mAh/g.

2-2. $LiMn_2O_4$

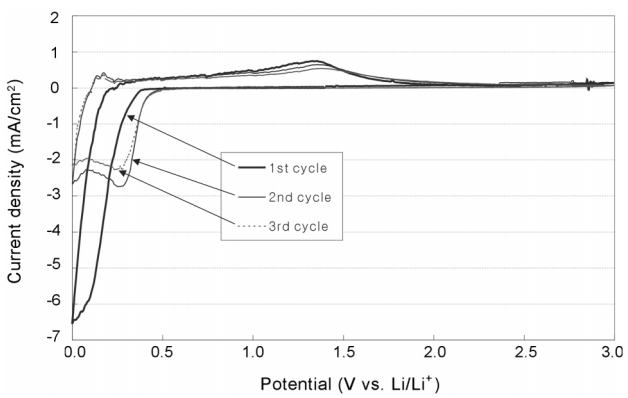

Fig. 9. Cyclic voltammogram of $LiMn_2O_4$/lithium cell. Scan rate; 0.1 mV/sec, potential range; 0-3 V vs Li/Li+.

Electrochemical characteristics of $LiMn_2O_4$ were also investigated by using the same technique as in $LiCoO_2$.

The Li|$LiMn_2O_4$ (singleside, 7 mg/cm^2) cell was tested with a scan rate of 0.1 mV/sec and potential range of 0-3 V vs. Li|Li$^+$ by cyclic voltammetry as shown in Fig. 9. During the 1st cathodic scan, the current increased continuously from ca. 0.4 V to 0 V with some different slope, indicating the existence of another reduction except for the lithium deposition. The current peak on the oxidation process was observed at 1.35 V as a corresponding peak to the reduction. After the 2nd cycle, the cathodic current started to increase at 0.5 V. Therefore, the cathodic process after the 2nd cycle was dif-

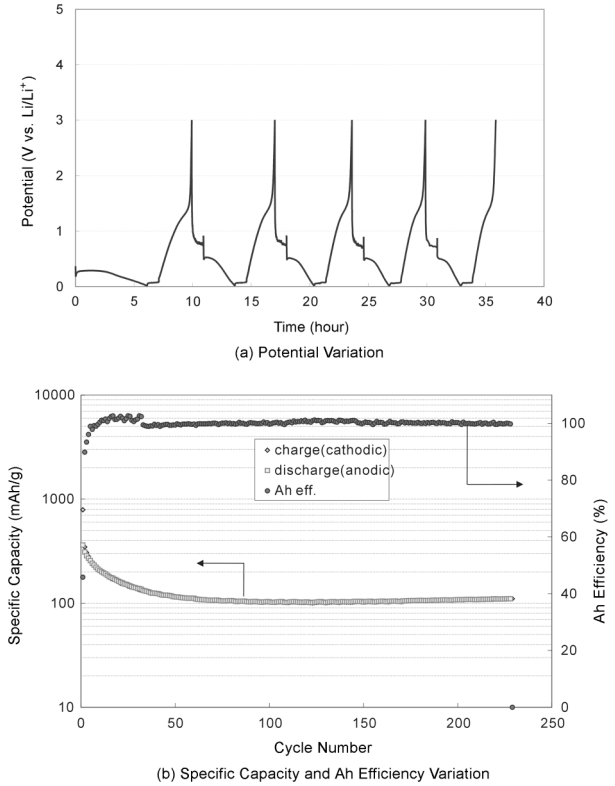

Fig. 10. Charge-discharge characteristics of $LiMn_2O_4$/lithium cell. Current density; 0.5 mA/cm^2, potential range; 0-3 V vs Li/Li$^+$, rest; 30 minutes.

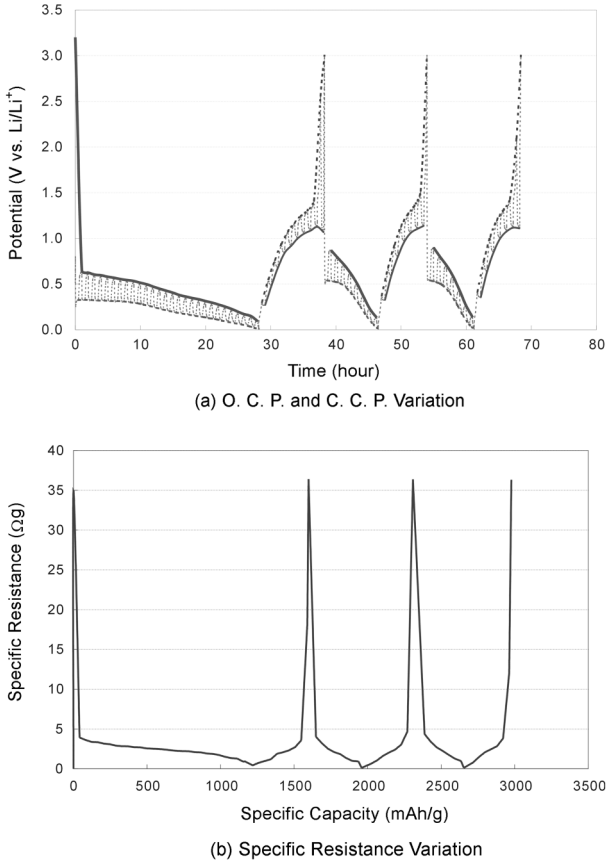

Fig. 11. Intermittent charge-discharge characteristics of $LiMn_2O_4$/lithium cell. Current density; 0.5 mA/cm^2, potential range; 0-3 V vs Li/Li$^+$, current on; 30 minutes, current off; 30 minutes, charge per one pulse; 41 mAh/g.

ferent from the one of the 1st cycle.

The cell properties of a fresh Li|$LiMn_2O_4$(Cu) cell were evaluated galvanostatically at a current density of 0.5 mA/cm^2 and potential range of 0.01-3 V by the charge-discharge tester. The result is shown in Fig. 10a. At the initial charge of the 1st cycle, the potential decreased rapidly from 3 V (O.C.P.) to 0.18 V and then it restored to 0.28 V, and a potential plateau, which was lower than that of $LiCoO_2$ (1.1 V), was observed. The potential decreased gradually while the charge proceeded. The specific capacity at the 1st charge was 790 mAh/g-$LiMn_2O_4$. The potential behavior of the discharge step was different from that of the charge step. The specific capacity at the 1st discharge was 362 mAh/g-$LiMn_2O_4$, so the Ah efficiency and the irreversible specific capacity of the 1st discharge were 46% and 428 mAh/g, respectively. The specific capacity of 362 mAh/g was similar to 372 mAh/g of graphite. The capacity density of $LiMn_2O_4$ was twice higher than the graphite because the density of $LiMn_2O_4$ was double that of the graphite. Average potential of the 2nd cycle was higher than that of the 1st cycle. Fig. 10b shows the specific capacity and the Ah efficiency plot as a function of charge-discharge cycling. The specific capacities decreased to 110 mAh/g at 130th cycle, and thereafter increased gradually. The Ah efficiencies were almost 100% as the result of reversible redox reaction.

A fresh Li|$LiMn_2O_4$ cell was tested to obtain the O.C.P. (bold line) and C.C.P. (dotted line) lines by using GITT as shown in Fig. 11a. The O.C.P. decreased gradually from 0.6 V to 0.1 V. Two ambiguous potential plateaus appeared. The O.C.P. pattern after the 1st discharge was different from the 1st charge and showed a reversible reaction. Fig. 11b shows the specific resistance plot as a function of the specific capacity obtained from the similar method in Fig. 7b. At the 1st charge of $LiCoO_2$, the specific resistance was 8 ohm·g in the irreversible region. But, in the case of $LiMn_2O_4$, the specific resistance went down gradually with increasing the specific capacity.

Fig. 12a shows results of the signature test of Li|$LiMn_2O_4$ cell. Fig. 12b shows the specific capacity plot, which was obtained by using the results of Fig. 12a, as a function of the specific current. The specific capacities were 150, 200, 300 and 360 mAh/g at the specific current of 700, 400, 80 and 30 mA/g, respectively. The specific capacity increased with decreasing the specific current. The specific capacity of $LiMn_2O_4$ was higher than that of Li|$LiCoO_2$ cell.

Charge-discharge results of $LiMn_2O_4$ for the 1st cycle are summarized in Table 4. The irreversible specific capacity of nos. 2-3 in Table 4, which contained 92 wt% $LiMn_2O_4$ in the electrode, was ca. 800 mAh/g. But that of no. 1, which contained 86 wt% $LiMn_2O_4$ in the electrode, was 428 mAh/g. The charge-discharge characteristics of STC-$LiMn_2O_4$ shown at nos. 4-6 in Table 4 were tested to compare with other electrode materials. The irreversible specific capacity of Li|STC-$LiMn_2O_4$ cell was also ca. 800 mAh/g. The specific discharge capacity of STC-$LiMn_2O_4$ was lower than that of AS-$LiMn_2O_4$, but their characteristics as the anode were almost the same.

3. Reaction Mechanism

In the Li|$LiCoO_2$ and Li|$LiMn_2O_4$ cell, the potential behavior at

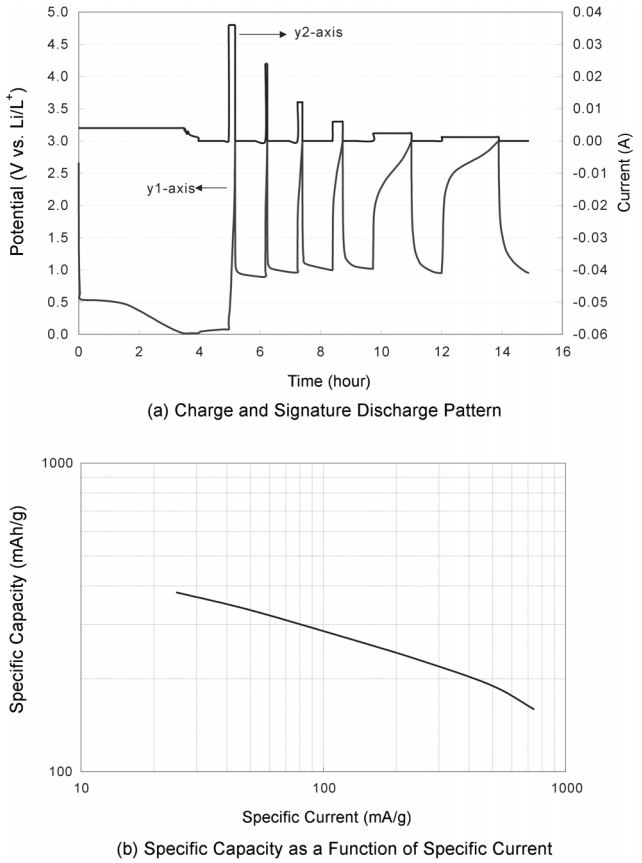

Fig. 12. Drain capability of $LiMn_2O_4$ cell obtained by using the signature discharge technique.

the 1st charge was different from that of the 2nd charge thereafter. This indicated that the reaction mechanism at the 1st charge was different from the further cycle. Tarascon et al. [Poizot et al., 2000] have recently reported that transition-metal oxide could be electrochemically reduced to nano-sized metal particles. Dahn et al. [Courtney and Dahn, 1997] have reported that electrochemical reduction of SnO_x produced metallic tin and lithium oxide. Our results of potential behavior were similar to that of Tarascon and Dahn. The reaction mechanism of LiTMO could be proposed as Eq. (1) and Eq. (2) based on the results of Tarascon and Dahn.

$$LiCoO_2 + 3Li^+ + 3e^- \Leftrightarrow 2Li_2O + Co^0 \quad (1)$$

$$LiMn_2O_4 + 7Li^+ + 7e^- \Leftrightarrow 4Li_2O + 2Mn^0 \quad (2)$$

Table 3. The Electrochemical characteristics of $LiCoO_2$[a]/Li cell at the 1st charge-discharge

No.	Current density (mA/cm^2)	Qc1 (mAh/g)	Qd1 (mAh/g)	Ah eff. (%)	Q_{irr} (mAh/g)
1	0.50	917	266	29.00	651
2	0.09	930	273	29.41	657
3	0.05	941	328	34.86	613

[a]Electrode composition of $LiCoO_2$, Lonza KS6 and PVDF was 83.3 : 12.5 : 4.2 wt%.

Theoretical specific capacities of $LiCoO_2$ and $LiMn_2O_4$ were 490 and 1,036 mAh/g based on a formula weight of 164 g and 181 g, respectively. In the case of $LiCoO_2$, the specific charge capacity was 917 mAh/g (no. 1 in Table 3), which exceeds theoretical value. The high specific charge capacity might have resulted from the irreversible solvent decomposition and/or Li-Co alloy formation. The specific capacity of $LiMn_2O_4$ at the 1st charge was 790 mAh/g (no. 1 in Table 4). That was 76.2% of the theoretical value. However, the reaction mechanism of LiTMO, which is directly related to the low initial Ah efficiency and the capacity fading by charge-discharge cycling, must be precisely studied.

CONCLUSION

The electrochemical properties of lithium transition-metal oxides (LiTMOs) such as $LiCoO_2$ and $LiMn_2O_4$ were evaluated as the anode for the lithium secondary battery. LiTMO had fairly good properties as an anode as well as a cathode.

At the 1st cathodic process, $LiCoO_2$ had a potential plateau at 1.4 V on an open circuit potential line, but $LiMn_2O_4$ had two ambiguous potential plateaus between 0.6-0.1 V on the open circuit potential line. The specific resistance of Li|$LiCoO_2$ cell was 8 ohm·g, but that of the Li|$LiMn_2O_4$ cell decreased gradually as the reaction proceeded.

The specific capacities of the Li|$LiCoO_2$ and Li|$LiMn_2O_4$ cells at the 1st discharge were about 300 mAh/g.

Capacity retention of Li|$LiMn_2O_4$ cell during the charge-discharge cycling was better than that of Li|$LiCoO_2$ cell. The specific capacity of Li|$LiMn_2O_4$ and Li|$LiCoO_2$ cells was 110 and 20 mAh/g at the 100th cycle, respectively.

The possibility of LiTMO as an anode material for lithium secondary battery could be confirmed. But a reduction of irreversible capacity and the enhancement of cycling property must be achieved

Table 4. The electrochemical characteristics of $LiMn_2O_4$/Li cell at the 1st charge-discharge

No.	Manufacture	Electrode composition (wt%)	Current density (mA/cm^2)	Q_{C1} (mAh/g)	Q_{D1} (mAh/g)	Ah eff. (%)	Q_{irr} (mAh/g)
1	AS	86 : 4 : 4 : 6[a]	0.50	790	362	45.84	428
2	AS	92 : 2 : 2 : 4[b]	1.0	1,063	252	23.706491	811
3	AS	92 : 2 : 2 : 4[b]	0.27	1,038	279	26.878613	759
4	STC	92 : 2 : 2 : 4[b]	1.0	917	103	11.232279	814
5	STC	92 : 2 : 2 : 4[b]	0.27	1,010	199	19.70297	811
6	STC	92 : 2 : 2 : 4[c]	1.0	835	63	7.56	772

a: SGO1 : SPB : PVDF, b: VGCF : SSB : PVDF, c: SGO1 : SPB : PVDF

for the commercialization of LiTMO as an anode.

REFERENCES

Courtney, I. A. and Dahn, J. R., "Key Factors Controlling the Reversibility of the Reaction of Lithium with SnO_2 and Sn_2BPO_6 Glass," *J. Electrochem. Soc*., **144**, 2943 (1997).

Dahn, J. R., Sleigh, A. K., Shi, H., Way, B. M., Weydanz, W. J., Reimers, J. N., Zhong, Q. and von Saken, U., "Carbons and Graphites as Substitutes for the Lithium Anode," Lithium Batteries, Ed. Pistoia, G., Elsevier, New York, 1 (1994).

Doh, C. H., Moon, S. I. and Yun, M. S., "Properties of $LiPF_6$ (PC+EC+DEC) Electrolyte by the Variation of PC Fraction and Initial Electrochemical Properties of Carbon Anode in the Electrolyte," *J. Korean Electrochem. Soc*., **3**, 224 (2000).

Doh, C. H., Moon, S. I., Yun, M. S. and Yum, D. H., "Initial Capacity Fading of Meso-Phase Pitch Based Carbon Fiber as Anode Material of Lithium Ion Battery," *Bull. Korean Chem. Soc*., **21**, 169 (2000).

Doh, C. H., Moon, S. I., Yun, M. S., Jin, C. S., Jin, B. S. and Eom, S. W., "Initial Electrochemical Insertion/Desertion of Lithium into Hard Carbon," *Carbon Science*, **1**, 36 (2000).

Doh, C. H., Moon, S. I., Yun, M. S., Park, C. J., Yum, D. H. and Yun, S. K., "Initial Charge/Discharge of $LiCoO_2$ Composite Cathode with Various Content of Conductive Material for the Lithium Ion Battery," *J. Korean Electrochem. Soc*., **2**, 123 (1999).

Dubois, M., Froyer, G. and Billaud, D., "Para-Sexiphenylene as a Model Compound of Poly(para-phenylene) During the Electrochemical Intercalation of Lithium and Sodium Ions in Ethylene Carbonate-Based Electrolyte," *Synth. Met*., **97**, 217 (1998).

Idota, Y., Matsufuji, A., Maekawa, Y. and Miyasaki, T., "Tin-Based Amorphous Oxide: A High-Capacity Lithium-Ion-Storage Material," *Science*, **276**, 1395 (1997).

Idota, Y., Mishima, M., Miyaki, Y., Kubotam T., Miyasaki, T. and Miyasaka, T., "Nonaqueous Secondary Battery," Eur. Pat. EP 0,651,450, A1 (1995).

Idota, Y., "Nonaqueous Secondary Battery," US5,478,671 (1995).

Poizot, P., Laruelle, S., Grugeon, S., Depont, L. and Tarascon, J.-M., "Nano-sized Transition-metal Oxides as Negative-Electrode Materials for Lithium-Ion Batteries," *Nature*, **407**, 496 (2000).

Sun, Y.-K. and Kim, D.-W., "Synthesis and Electrochemical Characterization of $LiMn_2O_4$ Cathode Materials for Lithium Polymer Batteries," *Korean J. Chem. Eng*., **16**, 449 (1999).

Sun, Y.-K., Kim, D.-W., Jin, S.-H., Hyung, Y.-E., Moon, S.-I. and Park, D.-K., "Synthesis and Cycling Behavior of $LiMn_2O_4$ Cathode Materials Prepared by Glycine-Assisted Sol-Gel Method for Lithium Secondary Batteries," *Korean J. Chem. Eng*., **15**, 64 (1998).

Yamabe, T., Tanaka, K., Ago, H., Yoshizawa, K. and Yata, S., "Structure and Properties of Deeply Li-Doped Polyacenic Semiconductor (PAS)," *Synth. Met*., **86**, 2411 (1997).